

EIRA Journal of Multidisciplinary Research and Development (EIRAJMRD)
Journal homepage: https://eirapublisher.com/eirajmrd/
Email: office.eirapublisher@gmail.com
ISSN: 3107-9350 (Online)
Volume 2, Issue 6, (November-December) 2026
DOI: https://doi.org/10.5281/zenodo.24149663

Implementation and Performance Evaluation of an Enhanced Bacteria Foraging Optimisation Algorithm for Feature-Level Fusion in Multibiometric Systems

Akinwumi A. R.[1]; Olabiyisi S. O.[2]; Oyeleye C. A.[3] & Odeniyi O. A.[4]

[1,2]Department of Computer Science, Ladoke Akintola University of Technology, Ogbomoso, Oyo State, Nigeria.
[3]Department of Information Science, Ladoke Akintola University of Technology, Ogbomoso, Oyo State, Nigeria.
[4]Department of Computer Science, Osun State College of Technology, Esa-Oke, Osun State, Nigeria.

Article history:
Received: 01/09/2026
Accepted: 15/10/2026
Published: 12/11/2026

Keywords: *multibiometric systems; feature-level fusion; bacteria foraging optimization; chemotaxis; elimination-dispersal; discrete wavelet transform; biometric database*

***Corresponding Author:**
Akinwumi A. R.

Copyright © 2026 The Author(s). This is an open-access article distributed under the terms of the Creative Commons Attribution-Noncommercial 4.0 International License (CC BY-NC 4.0)

Abstract **Original Research Article**

Feature-level fusion of multiple biometric traits retains more discriminative information than fusion at later stages, but it is difficult in practice: the concatenated feature vector is high-dimensional, features from different modalities are incompatible, and the search for a good combination is computationally expensive. The Bacteria Foraging Optimization Algorithm (BFOA) is an attractive search technique for this task, yet its fixed chemotaxis step size and constant elimination-dispersal probability slow convergence and let bacteria stagnate in local optima. This paper reports the design of a multimodal biometric database and the formulation of an Enhanced BFOA (EBFOA) for feature-level fusion. The database was acquired locally from 150 students and staff of OSCOTECH under uncontrolled conditions and contains 900 face, 1,800 iris (left and right eyes) and 1,800 fingerprint (left and right thumbs) images, six samples per subject per trait. Each modality was passed through a modality-specific preprocessing, normalisation and segmentation pipeline and reduced by a single-level Haar discrete wavelet transform to an eight-element feature vector. EBFOA modifies BFOA in two ways: the chemotaxis step size was drawn from [0, 1] instead of being fixed, and the elimination-dispersal probability was made dependent on fitness rank and elimination-dispersal cycle through linear and nonlinear forms. The formulation was implemented in MATLAB 2023a and is evaluated analytically. The probability profiles reduce to the constant probability of standard BFOA at the first cycle, increase monotonically with fitness rank, and increasingly protect the fittest bacteria while relocating the weakest; the added cost is O(S) arithmetic operations per cycle, which is negligible beside fitness evaluation. The paper provides a documented, reproducible database design and a precisely specified EBFOA on which empirical recognition studies can be built.

How to cite this article: Akinwumi A. R., Olabiyisi S. O., Oyeleye C. A., & Odeniyi O. A. (2026). Implementation and performance evaluation of an enhanced bacteria foraging optimisation algorithm for feature-level fusion in multibiometric systems. EIRA Journal of Multidisciplinary Research and Development, 2(6). 01-10.

1. Introduction

Reliable identity verification underpins banking, electronic commerce, access control and law enforcement, and biometric traits such as the face, fingerprint and iris are widely used because they are universal, measurable and difficult to transfer between people. Most deployed systems nevertheless rely on a single trait. A unimodal system is exposed to noisy sensor data, intra-class variation, non-universality and spoofing, and these weaknesses limit the accuracy it can reach in demanding applications (Jain et al., 2006; Ross et al., 2006). Multibiometric systems address them by combining evidence from several independent sources.

Evidence can be combined at the sensor, feature, score or decision level. Feature-level fusion is generally regarded as the most powerful because it operates on the richest information, before any matching decision discards it (Krishneswari & Arumugam, 2012; Awang et al., 2013). It is also the hardest to realise. Concatenating the feature vectors of several traits produces a high-dimensional vector (the curse of dimensionality); the feature spaces of different

modalities may be incompatible and their mutual relationship is usually unknown; and an arbitrary combination is unlikely to be optimal or to balance the contribution of each source (Dapinder & Gaganpreet, 2013; Nahdeen & Poornima, 2013). Searching for a good combination is a large, non-linear optimisation problem for which exhaustive and classical methods are poorly suited, which is why metaheuristics have been applied to it (Boussaïd et al., 2013; Adedeji et al., 2015).

The Bacteria Foraging Optimization Algorithm (BFOA) imitates the chemotaxis, swarming, reproduction and elimination-dispersal behaviour of *Escherichia coli* (Passino, 2002). It is easy to implement, insensitive to initialisation and good at exploitation, and has been applied to feature selection among many other problems (Chen et al., 2017; Guo et al., 2021). It also has well-documented weaknesses. The chemotaxis step size is a fixed constant, so the algorithm cannot simultaneously converge quickly and refine its solution accurately, and the constant elimination-dispersal probability can drive a bacterium away from an optimum it has already found (Li et al., 2014; Niu et al., 2015; Akinwumi et al.,). Performance also degrades as the dimensionality of the search space grows (Tang et al., 2007).

A second difficulty concerns evaluation data. Public biometric databases are usually captured in controlled environments and tailored to the algorithm they were built for, so reported performance changes when the dataset changes. A database that reflects realistic, uncontrolled acquisition, and that is documented well enough to be reproduced, is therefore a necessary companion to any new fusion algorithm.

This paper addresses both needs. Its contributions are:

i. **A multimodal biometric database design.** A locally acquired database of face, iris and fingerprint images from 150 subjects, with a documented acquisition protocol, modality-specific preprocessing, normalisation and segmentation, and a compact Haar-wavelet feature representation.

ii. **A formulation of EBFOA.** Two modifications of BFOA, a variable chemotaxis step size and a non-uniform, rank- and cycle-dependent elimination-dispersal probability, with the equations, parameter set and pseudocode needed to reproduce them.

iii. **An analytical evaluation of the formulation.** The properties of the elimination-dispersal schedule and the step-size distribution are derived and illustrated, and the computational overhead is bounded.

The remainder of the paper is organised as follows. Section 2 reviews related work. Section 3 describes the database design, the EBFOA formulation and its implementation. Section 4 presents and discusses the database properties and the analytical evaluation of EBFOA. Section 5 concludes.

2. Related Works

Feature-level fusion has been pursued with hand-crafted descriptors, learned representations and search-based selection. Deshmukh et al. (2013) fused face and fingerprint features extracted with a Gabor filter bank and used linear discriminant analysis and principal component analysis to control dimensionality, reporting a recognition accuracy of 99.25%. Bouzouina and Hamami (2017) combined face and iris, selecting iris features with a genetic algorithm and verifying users with a support vector machine (98.8% accuracy). Alshebli et al. (2021) merged discrete wavelet transform and singular value decomposition features of the face and iris into a single pattern per individual. Deep models have also been used: Soleymani et al. (2018) fused iris, face and fingerprint features at several levels of a convolutional network, and Sagar and Jain (2023) extracted fingerprint and iris features with convolutional networks for verification.

A smaller body of work treats fusion as an optimisation problem. Adedeji et al. (2015, 2021) applied the clonal selection algorithm and a modified version with neighbourhood tournament selection to face, iris and fingerprint fusion, and found that the modified algorithm gave higher recognition accuracy and lower recognition time. Jooda et al. (2021) used the artificial bee colony algorithm to select fingerprint features before classification, and Vensila and Boyed (2024) reduced fused finger-vein, face and fingerprint features with an adaptive particle swarm optimiser before an extreme learning machine. These studies indicate that swarm and evolutionary search can reduce dimensionality and improve fused-feature quality, but the choice of search algorithm and its convergence behaviour remain open.

Since Passino (2002), BFOA research has grown into a large literature, surveyed by Guo et al. (2021), who group the improvements into parameter adjustments, structure adjustments, hybrid strategies and individual-based models. Because the chemotaxis step length is the most critical user-defined parameter, many studies replace the fixed constant with a step that decreases over the run or adapts to the search state (Chen et al., 2008; Niu et al., 2015). Pang et al. (2019) drew step sizes from a Lévy-flight distribution that yields frequent small and occasional large moves, and combined it with a particle swarm operator; Wang et al. (2018) introduced a Gaussian chemotactic strategy in a bare-bones variant; and Tan et al. (2015) proposed an adaptive comprehensive-learning variant. Hybrids with differential evolution (Biswas et al., 2007) and particle swarm optimisation (Liang & Tian, 2017) improve convergence at the price of additional operators.

Comparatively less attention has been given to the elimination-dispersal operation. Li et al. (2014) observed that an elimination-dispersal step can make a bacterium that has found, or nearly found, an optimum escape from it, and suggested that its sphere of action be altered as the generations of the evolution advance. Applications of BFOA to feature selection exist (Chen et al., 2017), but BFOA-style search has seldom been applied to feature-level fusion of face, fingerprint and iris (Akinwumi et al.,).

Two gaps follow. First, feature-level fusion of face, fingerprint and iris is rarely evaluated on data acquired in an uncontrolled setting with a fully documented protocol. Second, the elimination-dispersal operation of BFOA, which governs the balance between protecting good solutions and escaping poor ones, is usually left as a constant. This paper responds by designing such a database and by formulating an EBFOA in which both the chemotaxis step and the elimination-dispersal probability vary.

3. Materials and Methods

3.1 Research framework

The work follows a pipeline in which each stage consumes the output of the previous one (Figure 1). Face, fingerprint and iris images are acquired, preprocessed, segmented and reduced to feature vectors. The feature vectors are concatenated and the fusion weights are searched by EBFOA. Implementation and recognition-performance experiments build on these two stages and are outside the scope of this paper.

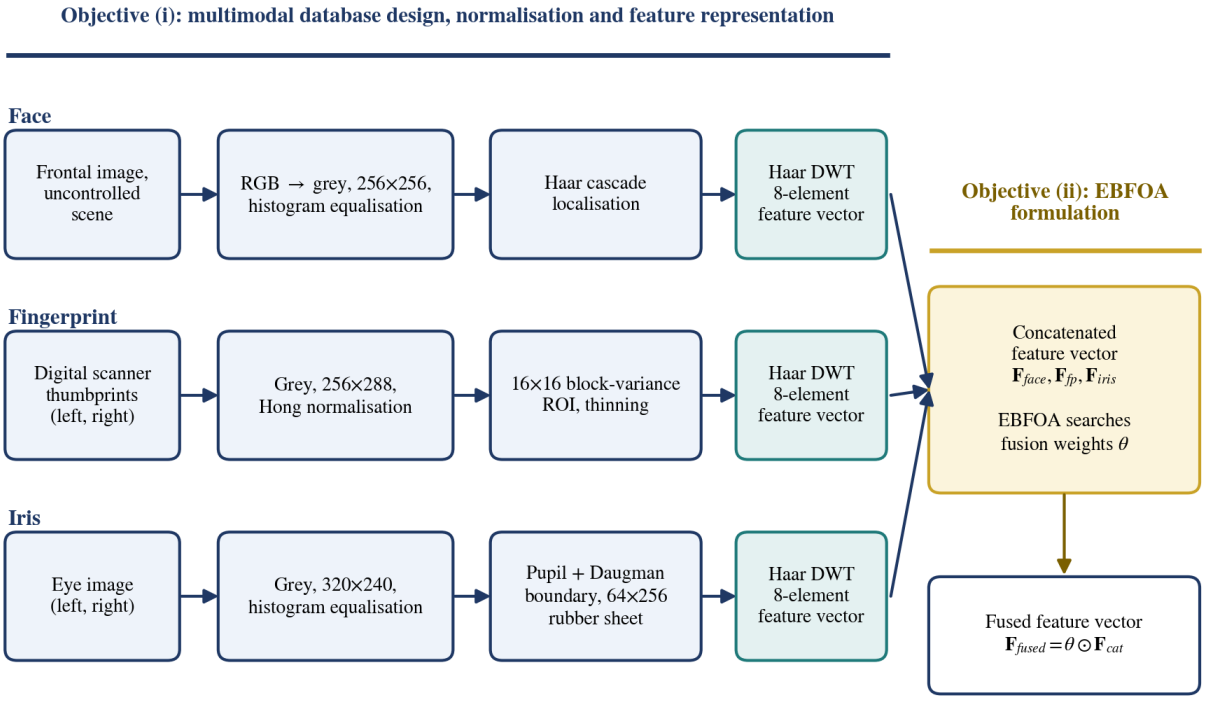


Figure 1. *Framework of the study: database design, normalisation and feature extraction for each modality, and EBFOA-based feature-level fusion.*

3.2 Design of the multimodal biometric database

The database was designed to reflect realistic, uncontrolled acquisition rather than the controlled conditions typical of public collections. Subjects were 150 students and staff of the Osun State College of Technology (OSCOTECH), Esa-Oke, selected at random. The same 150 individuals contributed all three traits, so every subject has face, iris and fingerprint data and any combination of the traits can be fused.

Face images were captured with a high-resolution CMITECH iris camera in an uncontrolled environment. All faces were frontal, with little variation in expression, illumination and subject-to-camera distance; six images were taken per subject, giving 900 images. Eye images, containing the iris, pupil, sclera, eyelids and eyelashes, were captured from the same subjects with the same camera. Both eyes were captured simultaneously to form a bi-instance iris database, stored in Left Iris and Right Iris folders of 900 images each (six images per subject per eye). Thumbprints were acquired with a digital personal fingerprint scanner, six impressions per thumb per subject, and stored in Left Thumb and Right Thumb folders of 900 grey-scale images each. The database therefore holds 4,500 images (Table 1).

Table 1. *Composition of the multimodal biometric database*

Modality	Acquisition device	Instances	Subjects	Samples per instance	Images	Native resolution
Face	CMITECH high-resolution iris camera	Frontal face	150	6	900	720 × 960
Iris	CMITECH iris camera	Left eye, right eye (bi-instance)	150	6	1,800 (900 + 900)	640 × 480
Fingerprint	Digital personal fingerprint scanner	Left thumb, right thumb	150	6	1,800 (900 + 900)	355 × 390
Total			**150**		**4,500**	

Raw images vary in illumination, sensor noise, scale and background, so the same operations were applied to every image of a given modality. Face images were acquired in colour and converted to 8-bit grey scale with the luminosity-weighted transformation in Equation (1), which reduces three channels to one and lowers the cost of later stages without discarding structural information. Iris and fingerprint images were captured directly in grey scale.

$$(I(x,y) = 0.299R(x,y) + 0.587G(x,y) + 0.114B(x,y) \qquad (1)$$

Because the three devices produce images of different native resolutions (Table 1), each modality was resized with bilinear interpolation to a fixed standard size: 256 × 256 pixels for the face, 320 × 240 for the iris and 256 × 288 for the fingerprint. This makes feature vectors the same length for every sample and spatially comparable. Illumination differences in face and iris images were reduced by histogram equalisation (Equation 2), in which L is the number of grey levels and $p_r(k)$ the probability of grey level k.

$$g(x,y) = \text{round}\left[(L-1)\sum_{k=0}^{f(x,y)} p_r(k)\right] \qquad (2)$$

Fingerprints are sensor-captured ridge images, so uneven finger pressure on the platen was handled with the normalisation of Hong et al. (1998), which maps each pixel intensity $I(x, y)$ to a desired mean M_0 and variance VAR_0 (Equation 3; the positive root is used where $I(x, y) > M$ and the negative root otherwise, with M and VAR the observed mean and variance). It standardises the grey-level range without altering the ridge-valley structure.

$$N(x,y) = M_0 \pm \sqrt{\frac{\text{VAR}_0\,(I(x,y)-M)^2}{\text{VAR}}} \qquad (3)$$

The face was localised with a Haar-cascade classifier (Viola & Jones, 2001); the bounding rectangle was cropped and resized to 256 × 256. For the iris, the pupillary boundary was first estimated by intensity thresholding and contour analysis of the darkest, most circular region near the image centre. The limbic boundary was found with Daugman's integro-differential operator (Equation 4; Daugman, 2004), which searches for the circle (x_0, y_0, r) along which the change in Gaussian-smoothed average intensity is greatest, restricted to the more reliably visible left and right arcs. A Hough circle transform was applied as a validation check. The annular iris between the two boundaries was then unwrapped into a fixed 64 × 256 strip with the rubber-sheet model (Equation 5), in which $(x_p(\theta), y_p(\theta))$ and $(x_i(\theta), y_i(\theta))$ are points on the pupillary and limbic boundaries in direction θ and $r \in [0, 1]$. This removes the effect of pupil dilation and imaging distance (Figure 2).

$$\max_{(r,x_0,y_0)} \left| G_\sigma(r) * \frac{\partial}{\partial r}\int_{r,x_0,y_0} \frac{I(x,y)}{2\pi r}\,ds \right| \qquad (4)$$

$$x(r,\theta) = (1-r)\,x_p(\theta) + r\,x_i(\theta)$$

$$y(r,\theta) = (1-r)\,y_p(\theta) + r\,y_i(\theta) \qquad (5)$$

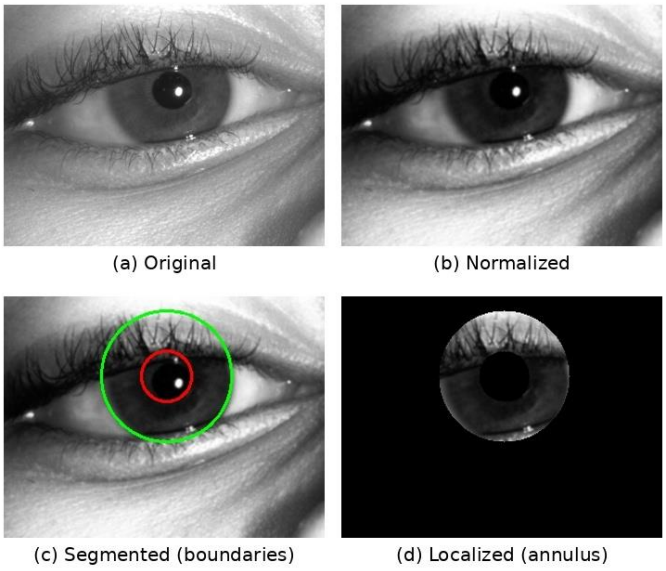


Figure 2. *Iris segmentation and localisation for a representative sample: original eye image, illumination-normalised image, detected pupillary and limbic boundaries, and isolated annular iris region.*

Fingerprint scans contain blank or noisy background where the finger is not in full contact with the platen, which would add spurious high-frequency content to the wavelet features. The normalised image was therefore divided into non-overlapping 16 × 16 blocks and the variance of each block computed (Equation 6, where M_k is the block mean and W the block width). Blocks whose variance fell below a fraction of the mean block variance were classed as background and removed from the region-of-interest mask, which was smoothed morphologically. Ridges within the region were enhanced, adaptively binarised and thinned to single-pixel skeletons (Figure 3).

$$V(k)=\frac{1}{W^2}\sum_{i=0}^{W-1}\sum_{j=0}^{W-1}(I(i,j)-M_k)^2 \tag{6}$$

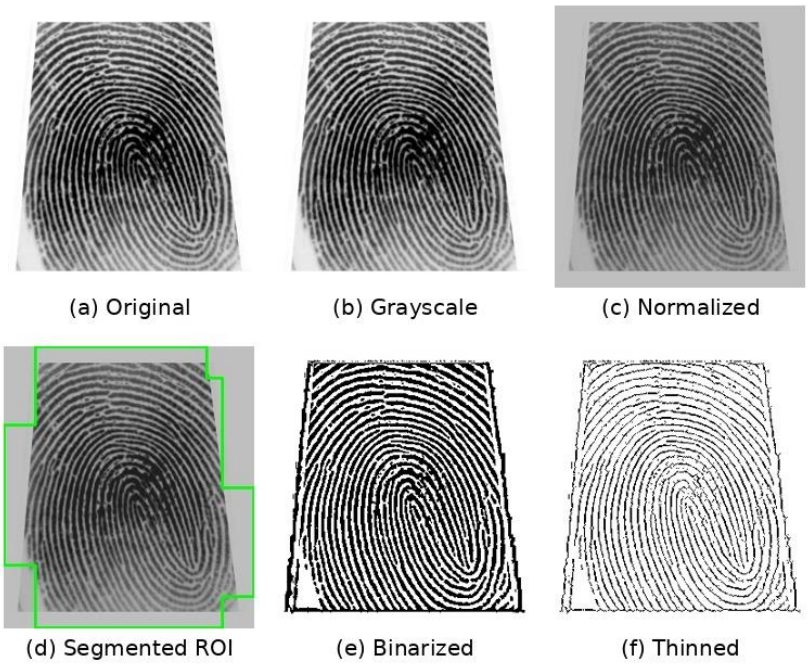


Figure 3. *Fingerprint segmentation and enhancement for a representative sample: original scan, grey-scale image, normalised image, segmented region of interest, binarised ridge-valley image and thinned ridge map.*

Features were extracted from the segmented face, the unwrapped iris strip and the normalised fingerprint with a single-level two-dimensional discrete wavelet transform (Mallat, 1989). The transform decomposes an image into an approximation subband (LL) and horizontal (LH), vertical (HL) and diagonal (HH) detail subbands (Equation 7). It was chosen because it captures spatial and frequency information jointly, and so represents the ridge, texture and edge structure that distinguishes one subject from another. The Haar wavelet was adopted for its simplicity and compact support. The mean (μ) and standard deviation (σ) of each subband were concatenated into the eight-element feature vector of Equation (8), one per modality.

$$W_{\varphi}(j_0,m,n)=\frac{1}{\sqrt{MN}}\sum_{x=0}^{M-1}\sum_{y=0}^{N-1}f(x,y)\,\varphi_{j_0,m,n}(x,y)$$

$$W_{\psi}^{q}(j,m,n)=\frac{1}{\sqrt{MN}}\sum_{x=0}^{M-1}\sum_{y=0}^{N-1}f(x,y)\,\psi_{j,m,n}^{q}(x,y),\quad q\in\{H,V,D\} \tag{7}$$

$$\mathbf{F}=[\mu_{LL},\,\sigma_{LL},\,\mu_{LH},\,\sigma_{LH},\,\mu_{HL},\,\sigma_{HL},\,\mu_{HH},\,\sigma_{HH}] \tag{8}$$

3.3 Formulation of the Enhanced Bacteria Foraging Optimization Algorithm

BFOA searches with a population of N bacteria through four processes (Passino, 2002). In chemotaxis a bacterium moves by tumbling, which picks a random direction, and by swimming, which continues in the same direction while fitness improves. Swarming lets bacteria signal one another through attractants and repellents. In reproduction, after N_c chemotactic steps, bacteria are ranked by accumulated fitness and the healthier half replaces the other half. In elimination-dispersal, each bacterium is eliminated with probability P_{ed} and a new bacterium is placed at a random position, which helps the swarm escape local optima. The parameters are listed in Table 2. In standard BFOA the step size $C(i)$ and the probability P_{ed} are fixed constants.

Let $\mathbf{F}_{face}$, $\mathbf{F}_{fp}$ and $\mathbf{F}_{iris}$ be the eight-element vectors of Equation (8). The position of a bacterium, θ, is a candidate fusion weight vector applied to their concatenation (Equation 9), and the fitness $J(i, j, k, l)$ of a bacterium is obtained by scoring the fused vector against the training partition of the database.

$$\mathbf{F}_{fused} = \theta \odot [\mathbf{F}_{face}, \mathbf{F}_{fp}, \mathbf{F}_{iris}] \tag{9}$$

In each chemotactic move the bacterium updates its position along a random unit direction (Equation 10), where $\Delta(i)$ is a random vector in $[-1, 1]^P$ and the term in the denominator normalises it to unit length, so the length of every move equals $C(i)$.

$$\theta^i(j+1, k, l) = \theta^i(j, k, l) + C(i)\frac{\Delta(i)}{\sqrt{\Delta^T(i)\,\Delta(i)}} \tag{10}$$

A fixed step forces a compromise: a large C converges quickly but may skip the optimum, and a small C is accurate but slow, which also raises computation time (Li et al., 2014). EBFOA replaces the constant with a variable step drawn from [0, 1] (Equation 11), so that fine and coarse moves are both available within the same chemotactic cycle and the swarm can explore and exploit without a manual choice of C.

$$C(i) \sim U(0, 1) \tag{11}$$

The elimination-dispersal probability p_e controls the balance between exploration and exploitation. A large value can destroy chemotactic progress but may relocate bacteria to better positions and avoid local minima; a small value preserves the best bacterium and intensifies local search, but gives it less chance of being released from a local minimum. EBFOA therefore assigns each bacterium a probability that depends on its fitness rank. After the chemotaxis steps the population is sorted by fitness and the first half is replicated into the second half (reproduction). A linear rank-dependent probability is then defined for $i = 1, 2, \ldots, S/2$, where S is the population size (Equation 12), and a nonlinear alternative squares it (Equation 13).

$$p_e(i) = \frac{i-1}{S/2-1}, \qquad i = 1, 2, \ldots, S/2 \tag{12}$$

$$p_e(i) = \left(\frac{i-1}{S/2-1}\right)^2, \qquad i = 1, 2, \ldots, S/2 \tag{13}$$

In both forms the fittest bacterium ($i = 1$) has probability 0 and the least fit ($i = S/2$) has probability 1, so the best solutions are protected and the worst are always relocated; the nonlinear form shifts probability mass towards the lowest ranks. Because the amount of exploration needed changes during the search, Equations (12) and (13) are generalised with the elimination-dispersal index $l = 1, 2, \ldots, N_{ed}$ and a base probability P_e ($0 \le P_e \le 1$) (Equations 14 and 15).

$$p_e(i, l) = P_e + \left[i - \left(\frac{S}{4} + 0.5\right)\right]\frac{l-1}{(N_{ed}-1)\,(S/2-1)} \tag{14}$$

$$p_e(i, l) = P_e\left[\frac{l-1}{N_{ed}-1}\right]\left[2\left(\frac{i-1}{S/2-1}\right)^2 - 1\right] + P_e \tag{15}$$

Writing x_i for the normalised rank and τ_l for the normalised cycle (Equation 16), the two forms simplify to Equation (17), which makes their behaviour transparent and is used in Section 4.2. Since p_e is a probability, computed values are bounded to [0, 1] (negative values are treated as 0 and values above 1 as 1).

$$x_i = \frac{i-1}{S/2-1}, \qquad \tau_l = \frac{l-1}{N_{ed}-1}, \qquad x_i, \tau_l \in [0, 1] \tag{16}$$

$$p_e^{lin}(i, l) = P_e + \tau_l\,(x_i - 0.5)$$

$$p_e^{non}(i, l) = P_e\left[1 + \tau_l\,(2x_i^2 - 1)\right] \tag{17}$$

Table 2. *Parameters of standard BFOA and their status in EBFOA*

Symbol	Description	Status in EBFOA
N	Number of bacteria, $i = 1, \ldots, N$	Unchanged
P	Dimension of the search space	Unchanged
N_c, N_{re}, N_{ed}, N_s	Numbers of chemotaxis, reproduction, elimination-dispersal and swim steps	Unchanged
$\Delta(i)$	Random tumble direction in $[-1, 1]$	Unchanged
$C(i)$	Chemotaxis step size of bacterium i	Modified: $C(i) \sim U(0, 1)$ replaces a fixed constant (Equation 11)
S	Population size used in the probability function ($S = N$)	Unchanged
P_e	Base elimination-dispersal probability, $0 \le P_e \le 1$	New: scales the non-uniform probability (Equations 14, 15)
P_{ed} / $p_e(i, l)$	Elimination-dispersal probability	Modified: rank- and cycle-dependent in place of a single constant
$J(i, j, k, l)$	Fitness of bacterium i at chemotaxis j, reproduction k, elimination-dispersal l	Unchanged (fusion objective)

Source: standard parameters after Passino (2002) and Biswas et al. (2007); modifications are those of this study.

Algorithm 1 gives the complete EBFOA. The two modifications are marked at steps 8 and 15; all other steps are those of standard BFOA.

Algorithm 1. Pseudocode of the Enhanced Bacteria Foraging Optimization Algorithm (EBFOA)

Step	Operation
1	Initialise N, P, N_c, N_{re}, N_{ed}, N_s, P_e and the bacterial positions θ^i
2	for $l = 1$ to N_{ed} // elimination-dispersal loop
3	for $k = 1$ to N_{re} // reproduction loop
4	for $j = 1$ to N_c // chemotaxis loop
5	for $i = 1$ to N
6	Compute fitness $J(i, j, k, l)$ of the fused vector (Equation 9); set $J_{last} = J(i, j, k, l)$
7	Generate random direction $\Delta(i)$
8	Modification 1: draw step size $C(i) \sim U(0, 1)$ (Equation 11)
9	Tumble: update $\theta^i(j+1, k, l)$ by Equation (10)
10	Swim: while $s < N_s$, if $J(i, j+1, k, l) < J_{last}$ then update J_{last} and move again, else set $s = N_s$
11	end for (next bacterium)
12	end for (until $j = N_c$)
13	Reproduction: sort bacteria by accumulated fitness; the healthier half replaces the other half
14	end for (until $k = N_{re}$)
15	Modification 2: for $i = 1, \ldots, S/2$ compute $p_e(i, l)$ from Equation (14) (linear) or (15) (nonlinear), bounded to [0, 1]
16	If rand() $< p_e(i, l)$, eliminate bacterium i and disperse it to a random position in the search space
17	end for (until $l = N_{ed}$)
18	Return the best position found (the fusion weight vector)

3.4 Implementation environment

EBFOA and standard BFOA were programmed in MATLAB 2023a on an Intel Core i3-7100 processor at 2.50 GHz with 4 GB of RAM running a 32-bit Windows 7 platform. The MATLAB core language implements the chemotaxis, reproduction and elimination-dispersal loops and the fitness function; the Image Processing Toolbox supports preprocessing, Hough-based iris segmentation and rubber-sheet normalisation; the Wavelet Toolbox computes the DWT coefficient matrices; the Statistics and Machine Learning Toolbox computes performance measures; and App Designer provides a graphical interface for selecting the modality configuration and the algorithm. A prototyping model was followed: a baseline BFOA fusion module was built first and the two modifications were then introduced and tested against it one at a time, so that EBFOA and BFOA can be run side by side on identical inputs.

4. Results and Discussion

The database holds 4,500 images from 150 subjects (Table 1): 900 face images, 1,800 iris images and 1,800 fingerprint images. Every subject has six samples of each trait instance, so up to 15 distinct genuine pairings per subject and instance can be formed (2,250 per instance across the 150 subjects). The bi-instance iris and bi-thumb structure allows left and right instances to be treated separately or together.

After normalisation, every image of a modality has the same size and the same eight-element descriptor, so the feature vectors of any modality are directly comparable and can be concatenated without further alignment. The seven fusion configurations, three unimodal, three bimodal and one trimodal, differ only in which descriptors are concatenated (Table 3), which allows the contribution of each trait, and of fusion itself, to be isolated on identical subjects.

Table 3. *Fusion configurations and fused feature-vector length*

Configuration	Modalities concatenated	Feature-vector length
Unimodal (3)	Face; Fingerprint; Iris	8 each
Bimodal (3)	Face + Fingerprint; Face + Iris; Fingerprint + Iris	16 each
Trimodal (1)	Face + Fingerprint + Iris	24

Three design choices distinguish the database from many public collections. Images were acquired in an uncontrolled environment, so illumination, background and pose vary as they would in a deployed system. The preprocessing pipeline is modality-specific yet fully specified, from colour conversion and resizing to segmentation parameters, so it can be reproduced. And one subject population supplies all traits, so any fusion combination can be evaluated without pairing traits from different people. Its limits are equally clear: all subjects come from a single institution, faces are frontal only, and no spoofing samples are included.

4.2 Analytical evaluation of the EBFOA formulation

The formulation was evaluated analytically, by deriving the properties of the elimination-dispersal schedule from Equations (12) - (17) and the step-size distribution from Equation (11). Figure 4 and Table 4 illustrate the schedule for a swarm of $S = 20$ bacteria (ranks $i = 1, \ldots, 10$), $N_{ed} = 4$ cycles and $P_e = 0.25$.

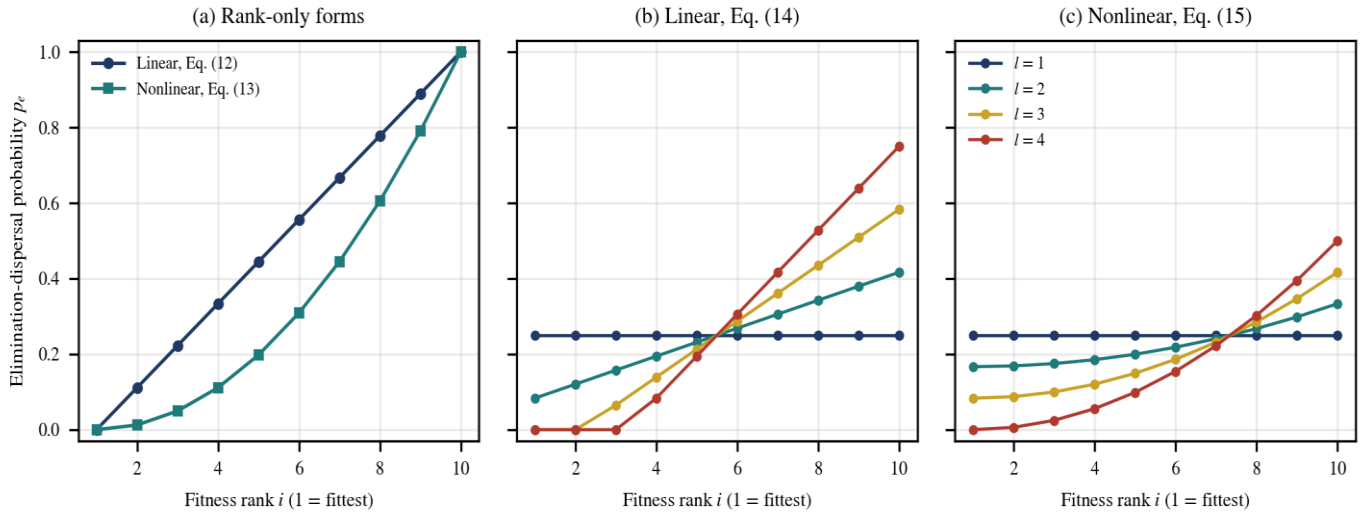


Figure 4. *Elimination-dispersal probability against fitness rank for $S = 20$, $N_{ed} = 4$ and $P_e = 0.25$: (a) rank-only forms, Equations (12) and (13); (b) linear form, Equation (14); (c) nonlinear form, Equation (15), for cycles $l = 1$ to 4. Values are bounded to [0, 1].*

Table 4. *Elimination-dispersal probabilities for the fittest (i = 1) and least fit (i = 10) bacteria, and expected number of bacteria dispersed per cycle (S = 20, N_{ed} = 4, P_e = 0.25)*

Cycle *l*	Linear: fittest	Linear: least fit	Linear: expected dispersed	Nonlinear: fittest	Nonlinear: least fit	Nonlinear: expected dispersed
1	0.25	0.25	2.50	0.25	0.25	2.50
2	0.08	0.42	2.50	0.17	0.33	2.25
3	0.00	0.58	2.59	0.08	0.42	2.01
4	0.00	0.75	2.92	0.00	0.50	1.76

Expected dispersed = sum of $p_e(i, l)$ over the ten ranks, after bounding to [0, 1]. Computed directly from Equations (14) and (15).

Property 1: reduction to standard BFOA. At the first cycle ($l = 1$) the factor τ_l in Equation (17) is zero, so $p_e(i, 1) = P_e$ for every rank in both forms. EBFOA therefore starts as BFOA with $P_{ed} = P_e$, and departs from it only as the cycles advance. This is visible in Figure 4(b) and 4(c), where the $l = 1$ curve is flat at 0.25.

Property 2: rank monotonicity. For any cycle after the first, p_e increases with i in both forms, because x_i and x_i^2 are increasing in i on [0, 1] and $\tau_l > 0$. The fittest bacteria are therefore always the least likely to be eliminated and the least fit the most likely, as intended.

Property 3: spread grows with the cycle. For the linear form, $p_e = P_e + \tau_l(x_i - 0.5)$, so the mean over ranks stays at P_e while the spread between the fittest and least fit grows linearly with τ_l, reaching $P_e \pm 0.5$ at the last cycle. In Table 4 the probability for the fittest bacterium falls from 0.25 to 0 and that of the least fit rises from 0.25 to 0.75. The nonlinear form, $p_e = P_e[1 + \tau_l(2x_i^2 - 1)]$, ranges from 0 to $2P_e$ at the last cycle, with a mean over ranks that falls towards about two thirds of P_e (the expected number dispersed falls from 2.50 to 1.76 in Table 4). Dispersal pressure thus becomes progressively concentrated on the weakest solutions, and total pressure under the nonlinear form decreases as the search matures, which favours exploitation late in the run.

Property 4: bounding. The linear form can fall below 0 for fit bacteria when $P_e < 0.5$, and the nonlinear form can exceed 1 when $P_e > 0.5$; the bounding to [0, 1] stated in Section 3.3.4 handles both. The slight rise in expected dispersals for the linear form in Table 4 (2.50 to 2.92) is an effect of that bounding at 0.

Property 5: step-size distribution. With $C(i) \sim U(0, 1)$ the expected step is 0.5 with variance 1/12, and 10% of moves are shorter than 0.1 and 10% longer than 0.9. Because the direction is normalised (Equation 10), each move has length exactly $C(i)$, so every chemotactic cycle mixes fine-grained refinement with long exploratory moves. A fixed C offers one of these behaviours at a time.

4.3 Computational cost

The additional work in EBFOA is small. Drawing $C(i)$ costs one random number per move, as in BFOA, which also draws a random direction. Evaluating $p_e(i, l)$ requires $O(S/2)$ arithmetic operations per elimination-dispersal cycle, so $O(N_{ed}S)$ over a run. The dominant cost in both algorithms is fitness evaluation, which is incurred $N \times N_c \times N_{re} \times N_{ed}$ times and each time requires scoring the fused vector against the training partition. The relative overhead of the modification is thus of the order $1/(N_{re}\, N_c\, C_J)$, where C_J is the cost of one fitness evaluation, and is negligible. The sorting needed to rank bacteria is already performed for reproduction.

4.4 Discussion

The database and the formulation are designed to complement each other. The database provides realistic, standardised, low-dimensional descriptors of three traits, and EBFOA provides a search procedure for combining them whose two modifications target the weaknesses of BFOA noted in the literature: the fixed step (Li et al., 2014; Niu et al., 2015) and the constant elimination-dispersal probability (Li et al., 2014). The step-size modification is related to adaptive and Lévy-flight step strategies (Chen et al., 2008; Pang et al., 2019) but is simpler, since no schedule or state variable is required. The elimination-dispersal modification is consistent with the suggestion of Li et al. (2014) that the operation should be adjusted as the evolution proceeds, and adds a dependence on fitness rank, so that protection is concentrated on the best solutions and relocation on the worst.

Two points deserve care. First, the step size is random rather than scheduled: Equation (11) does not decrease the step over the run, so the transition from exploration to exploitation arises mainly from the elimination-dispersal schedule and from the selection pressure of reproduction. A decaying upper bound on $C(i)$ would be a natural extension. Second, the benefit of both modifications is argued here from their mathematical properties. Whether they improve convergence

speed, recognition accuracy or error rates relative to standard BFOA is an empirical question that depends on the classification stage, decision thresholds and parameter settings; it is not claimed in this paper and requires the performance study that builds on this work.

The practical implications are, first, that other researchers can reproduce the pipeline and construct comparable databases from the documented protocol and, second, that the fusion search can be run unchanged for unimodal, bimodal and trimodal configurations, since only the length of the concatenated vector changes.

5. Conclusion

This paper presented a multimodal biometric database of face, iris and fingerprint images from 150 subjects, acquired in an uncontrolled environment and reduced to compact Haar-wavelet descriptors through a documented preprocessing, normalisation and segmentation pipeline, and formulated an Enhanced Bacteria Foraging Optimization Algorithm for feature-level fusion. EBFOA draws the chemotaxis step from [0, 1] and replaces the constant elimination-dispersal probability with linear and nonlinear forms that depend on fitness rank and cycle. Analysis showed that the formulation reduces to standard BFOA at the first cycle, protects the fittest bacteria and relocates the weakest with a spread that grows over the run, and adds negligible computational cost.

Future work will measure the recognition performance of EBFOA-based unimodal, bimodal and multimodal systems against standard BFOA, study the sensitivity of the results to P_e, N_{ed} and swarm size, examine a decaying bound on the chemotaxis step, and extend the database with more sessions, institutions and demographic variety.

References

1. Adedeji, O. T., Amusan, E. A., Alade, O. M., & Fenwa, O. D. (2021). Feature level fusion of biometric images using modified clonal selection algorithm. International Journal of Research and Review, 8(9). https://doi.org/10.52403/ijrr.20210965
2. Adedeji, O. T., Falohun, A. S., Alade, O. M., Omidiora, E. O., & Olabiyisi, S. O. (2015). Development of a modified clonal selection algorithm for feature level fusion of multibiometric systems. *LAUTECH Journal of Engineering and Technology, 9*(2), 80–85.
3. Akinwumi A. R., Olabiyisi S. O., Oyeleye C. A. & Odeniyi O. A. (2026). Towards the development of an enhanced bacteria foraging optimisation algorithm for feature-level fusion in multibiometric systems: A systematic literature review. UKR Journal of Multidisciplinary Studies (UKRJMS), 2(9): pp. 75 - 83 *https://doi.org/10.5281/zenodo.22810574*
4. Alshebli, S., Kurugollu, F., & Shafik, M. (2021). Multimodal biometric recognition using iris and face features. In *Advances in Manufacturing Technology XXXIV*. IOS Press. https://doi.org/10.3233/ATDE210045
5. Awang, S., Yusof, R., Zamzuri, M. F., & Arfa, R. (2013). Feature level fusion of face and signature using modified feature selection technique. In *Proceedings of the International Conference on Signal-Image Technology and Internet Based Systems* (pp. 706–713). IEEE Computer Society.
6. Biswas, A., Dasgupta, S., Das, S., & Abraham, A. (2007). A synergy of differential evolution and bacterial foraging optimization for global optimization. *Neural Network World, 17*(6), 607–626.
7. Boussaïd, I., Lepagnot, J., & Siarry, P. (2013). A survey on optimization metaheuristics. *Information Sciences, 237*, 82–117.
8. Bouzouina, Y., & Hamami, L. (2017). Multimodal biometric: Iris and face recognition based on feature selection of iris with GA and scores level fusion with SVM. In *Proceedings of the International Conference on Bio-engineering for Smart Technologies* (pp. 1–7).
9. Chen, H., Zhu, Y., & Hu, K. (2008). Self-adaptation in bacterial foraging optimization algorithm. In *Proceedings of the 3rd International Conference on Intelligent System and Knowledge Engineering* (pp. 1026–1031). IEEE.
10. Chen, Y. P., Li, Y., Wang, G., Zheng, Y. F., Xu, Q., Fan, J. H., & Cui, X. T. (2017). A novel bacterial foraging optimization algorithm for feature selection. *Expert Systems with Applications, 83*, 1–17.
11. Dapinder, K., & Gaganpreet, K. (2013). Level of fusion in multimodal biometrics: A review. *International Journal of Advanced Research in Computer Science and Software Engineering, 3*(2), 242–246.
12. Daugman, J. (2004). How iris recognition works. *IEEE Transactions on Circuits and Systems for Video Technology, 14*(1), 21–30.
13. Deshmukh, A., Pawar, S., & Joshi, M. (2013). Feature level fusion of face and fingerprint modalities using Gabor filter bank. In *Proceedings of the IEEE International Conference on Signal Processing, Computing and Control* (pp. 1–5).
14. Guo, C., Tang, H., Niu, B., & Lee, C. B. P. (2021). A survey of bacterial foraging optimization. *Neurocomputing, 452*, 728–746.

15. Hong, L., Wan, Y., & Jain, A. (1998). Fingerprint image enhancement: Algorithm and performance evaluation. *IEEE Transactions on Pattern Analysis and Machine Intelligence, 20*(8), 777–789.

16. Jain, A. K., Ross, A., & Pankanti, S. (2006). Biometrics: A tool for information security. *IEEE Transactions on Information Forensics and Security, 1*(2), 125–143.

17. Jooda, J. O., Oke, A. O., Omidiora, E. O., Adedeji, O. T., & Makinde, B. O. (2021). Fingerprint intramodal biometric system based on ABC feature fusion. *Asian Journal of Research in Computer Science, 11*(2), 1–10.

18. Krishneswari, K., & Arumugam, S. (2012). Multimodal biometrics using feature fusion. *Journal of Computer Science*.

19. Li, J., Dang, J., Bu, F., & Wang, J. (2014). Analysis and improvement of the bacterial foraging optimization algorithm. *Journal of Computing Science and Engineering, 8*(1), 1–10.

20. Liang, Y., & Tian, H. (2017). An improved hybrid algorithm based on bacterial foraging and particle swarm optimization. *Electronic Science and Technology*.

21. Mallat, S. G. (1989). A theory for multiresolution signal decomposition: The wavelet representation. *IEEE Transactions on Pattern Analysis and Machine Intelligence, 11*(7), 674–693.

22. Nahdeen, F. M., & Poornima, S. (2013). Feature level fusion in multimodal biometric authentication system. *International Journal of Computer Applications, 69*(18), 36–40.

23. Niu, B., Wang, J., & Wang, H. (2015). Bacterial-inspired algorithms for solving constrained optimization problems. *Neurocomputing, 148*, 54–62.

24. Pang, B., Song, Y., Zhang, C., Wang, H., & Yang, R. (2019). Bacterial foraging optimization based on improved chemotaxis process and novel swarming strategy. *Applied Intelligence, 49*(4), 1283–1305.

25. Passino, K. M. (2002). Biomimicry of bacterial foraging for distributed optimization and control. *IEEE Control Systems Magazine, 22*(3), 52–67.

26. Ross, A. A., Nandakumar, K., & Jain, A. K. (2006). *Handbook of multibiometrics*. Springer.

27. Sagar, P., & Jain, A. (2023). MultiNet: A multimodal approach for biometric verification. In *Computer Vision and Machine Intelligence: Proceedings of CVMI 2022* (pp. 679–690). Springer Nature Singapore.

28. Soleymani, S., Dabouei, A., Kazemi, H., Dawson, J., & Nasrabadi, N. M. (2018). Multi-level feature abstraction from convolutional neural networks for multimodal biometric identification. In *Proceedings of the 24th International Conference on Pattern Recognition* (pp. 3469–3476). IEEE.

29. Tan, L., Lin, F., & Wang, H. (2015). Adaptive comprehensive learning bacterial foraging optimization and its application on vehicle routing problem with time windows. *Neurocomputing, 151*, 1208–1215.

30. Tang, W., Wu, Q., & Saunders, J. (2007). A bacterial swarming algorithm for global optimization. In *Proceedings of the 2007 IEEE Congress on Evolutionary Computation* (pp. 1207–1212). IEEE.

31. Vensila, C., & Boyed, W. (2024). Multimodal biometrics authentication using extreme learning machine with feature reduction by adaptive particle swarm optimization. *The Visual Computer, 40*(3), 1383–1394.

32. Viola, P., & Jones, M. (2001). Rapid object detection using a boosted cascade of simple features. In *Proceedings of the 2001 IEEE Computer Society Conference on Computer Vision and Pattern Recognition* (Vol. 1, pp. 511–518). IEEE.

33. Wang, L., Zhao, W., Tian, Y., & Pan, G. (2018). A bare bones bacterial foraging optimization algorithm. *Cognitive Systems Research, 52*, 301–311.